Robust Geometric Phase of Bloch Sphere Deformation in Quasiphase Matched Structures

Feiyan Zhao, Haojun Zhang, Xiaoxi Xu, Huancan Liang, Hexiang He, Yangui Zhou, Jiantao Lü, and Yongyao Li

***Abstract*—We consider the adiabatic geometric phase (AGP) in the sum frequency generation process under the undepleted pump approximation. The Bloch sphere is stretched or compressed by adjusting the modulation wave vector, Δ, which is one of the control parameters of quasiphase matching (QPM). In this paper, two kinds of parametric rotation schemes on the sphere are studied: elliptical rotation and elliptical wedge rotation. We find that the AGP generated in the elliptical rotation is related to the length of the Δ axis of the ellipse, but there is a certain point where the AGP is independent, while the AGP in the elliptical wedge rotation shows great stability and does not depend on the shape of the ellipsoid. The results further demonstrate the superior flexibility of the wedge scheme, which helps to suppress the uncertainty in the generation of AGPs.**

***Index Terms*—Geometric phase, sum frequency generation, quasiphase matching.**

I. Introduction

NONLINEAR frequency conversion is an important technology to broaden the range of the laser spectrum and plays an important role in the development of highly efficient coherent light sources. It is well known that it is necessary to compensate for the wave vector mismatch to obtain high frequency conversion efficiency. In gas materials [1], [2], the refractive index can be changed by material ionization to meet the phase matching. However, crystals or waveguides cannot withstand super ionization, so phase matching based on ionization is not suitable. At present, the two most commonly used techniques in crystal materials are birefringence phase matching [3], [4] and quasiphase matching (QPM) [5]–[9]. Birefringence phase matching is carried out by using the constructive interference between signals [1]. This approach mixes different polarization states but may introduce unnecessary deviation between the interacting beams [10]. QPM technology can change the crystal structure periodically on the micron scale [11], and its high conversion efficiency and broadband robustness [12], [13] make it of wide concern. Optical frequency conversion in second-order and third-order nonlinear crystals using the QPM technique has caused extensive research, such as white femtosecond lasers [14], [15], infrared light sources [16], [17], ultrawideband chirped pulse amplifiers [18], and higher-order harmonic generation [19]–[22].

In the past decade, adiabatic frequency conversion [23] has developed rapidly due to its superiority in terms of bandwidth, efficiency and robustness. And it is more and more closely related to adiabatic geometric phase (AGP) in quantum mechanics. When the parameters of the Hamiltonian slowly transport along a circular trajectory, the quantum system in an eigenstate will obtain a geometric phase factor in addition to the inherent dynamic phase [24]. The phase factor is widely used for tunable beam switching [25], reconfigurable holography [26], beam shaping [27]–[29], optical data storage and communication [30], optical amplification [31], and so on. In the field of nonlinear frequency conversion, by using QPM technology, the input beams periodically polarize along the nonlinear crystal and accumulate AGPs. Karnieli and Arie [32] found that in the sum frequency generation (SFG) of the undepleted pump approximation, a controllable AGP can be accumulated when the QPM parameters rotate around the surface of the Bloch sphere. Then, based on this theory, they realized nonreciprocal transmission and wavefront shaping experimentally [33]. Recently, an accurate method [34] for calculating the AGP of pump depletion was proposed. This method is also applicable to the case of the undepleted pump and has been extended to calculate the AGP in the process of four wave mixing [35]. Based on this method, Ref. [36] found a constant AGP under different pump depletion levels in three wave mixing, while the other locations show a noticeable light intensity dependence. This light intensity dependent geometric phase can be used to rotate the local optical axis and modulate

Manuscript received April 20, 2022; revised May 19, 2022; accepted May 20, 2022. Date of publication May 24, 2022; date of current version June 3, 2022. This work was supported in part by NNSFC (China) under Grants 11905032 and 11874112, in part by the Natural Science Foundation of Guangdong province under Grant 2021A1515010214, in part by the Guangdong Basic and Applied Basic Research Foundation under Grant 2021A1515111015, in part by the Key Research Projects of General Colleges in Guangdong Province under Grant 2019KZDXM001, in part by the Foundation for Distinguished Young Talents in Higher Education of Guangdong under Grants 2018KQNCX279 and 2018KTSCX241, in part by the Special Funds for the Cultivation of Guangdong College Students Scientific and Technological Innovation under Grant pdjh2021b0529 and pdjh2022a0538, in part by the Research Fund of Guangdong-Hong Kong-Macao Joint Laboratory for Intelligent Micro-Nano Optoelectronic Technology under Grant 2020B1212030010, and in part by the Graduate Innovative Talents Training Program of Foshan University. *(Feiyan Zhao and Haojun Zhang contributed equally to this work.) (Corresponding author: Jiantao Lü.)*

Feiyan Zhao, Haojun Zhang, Xiaoxi Xu, Huancan Liang, and Jiantao Lü are with the School of Physics and Optoelectronic Engineering, Foshan University, Foshan 528000, China (e-mail: feiyanzhao@foxmail.com; 1969742727@qq.com; xu-xiao-xi@qq.com; 1762500586@qq.com; keentle@gmail.com).

Hexiang He, Yangui Zhou, and Yongyao Li are with the School of Physics and Optoelectronic Engineering, Foshan University, Foshan 528000, China, and also with the Guangdong-Hong Kong-Macao Joint Laboratory for Intelligent Micro-Nano Optoelectronic Technology, Foshan University, Foshan 528000, China (e-mail: hehx@mail2.sysu.edu.cn; zygsai@163.com; yongyaoli@gmail.com).

Digital Object Identifier 10.1109/JPHOT.2022.3177687

This work is licensed under a Creative Commons Attribution 4.0 License. For more information, see https://creativecommons.org/licenses/by/4.0/

the self-focusing transport of light in the medium [37]. Very recently, a new scheme of wedge rotation [38] in second-order nonlinear frequency was proposed. Moreover, the adiabatic and nondiabatic variations in the QPM parameters play an important role in whether the geometric phase is dependent on the pump depletion levels. However, to date, all the proposed rotation schemes have been carried out on the surface of the sphere. When the Bloch sphere is compressed or stretched, can these results be applied to this case? This is a question worth studying.

Based on this question, in this paper, we study the AGP accumulated when QPM vectors follow a closed trajectory on the ellipsoid in the undepleted pump approximation. The Bloch sphere is longitudinally compressed or stretched by adjusting the modulation wave vector, Δ. Two rotation schemes, elliptical rotation and elliptical wedge rotation, are compared. We find that the AGP in the elliptical rotation scheme depends on the shape of the sphere, but all the curves intersect to the same point; that is, there is a special value at which the AGP is independent of the shape of the sphere. The result in elliptical wedge rotation shows a gratifying stability. Regardless of how the long axis of the sphere changes, the accumulation of the AGP does not change, which effectively eliminates the uncertainty of generating AGPs in nonlinear frequency conversion. The rest of this paper is structured as follows. The calculation principle of the AGP in three-wave mixing with an undepleted pump approximation is briefly described in Section II. In Section III, we present the representation of two trajectories and discuss the main results of the AGP in elliptical and elliptical wedge rotation. The paper is summarized in Section IV.

II. Model and Principle

The coupled wave equations (CWEs) of the sum frequency with a slowly varying envelope, undepleted pump field and diffraction-free propagation are given by [5]:

$$\partial_z A_i = i\frac{2d(z)\omega_i}{cn_i}A_p^* A_s e^{-i\Delta k_0 z} \tag{1}$$

$$\partial_z A_s = i\frac{2d(z)\omega_s}{cn_s}A_p A_i e^{i\Delta k_0 z} \tag{2}$$

where $A_{i,p,s}$ are the slowly varying envelopes of the idler, pump and signal waves, respectively; $\Delta k_0 = k_i + k_p - k_s$ is the phase mismatch; and $d(z)$ is the spatial variation amplitude of the second-order nonlinear susceptibility applied with adiabatic modulation, which can be expanded by the Fourier series with slowly varying components as:

$$d(z) = d_{ij}\sum_{m=-\infty}^{\infty}|d_m(z)| \times e^{im[\int_0^z K_\Lambda(z')dz' + \phi_d(z)]}$$

with

$$d_m(z) = \begin{cases} (2/m\pi)\sin[m\pi D(z)] & m \neq 0 \\ 2D(z) - 1 & m = 0 \end{cases} \tag{3}$$

where d_{ij} is the corresponding nonlinear susceptibility tensor. $K_\Lambda(z)$, $0 < D(z) < 1$ and $\phi_d(z)$ are three QPM parameters, which represent the modulation wave vector, duty cycle, and phase factor of the modulation, respectively. In (3), only the terms of $m = \pm 1$ can provide the best compensation for the phase mismatch, and other terms can be dropped from the expansion.

We use the rotating wave approximation [32], which characterises the transformations from $A_{i,s}$ to $q_{i,s}$.

$$\begin{aligned} q_i &= \sqrt{\frac{n_i}{\omega_i}}e^{\frac{i}{2}\left[\Delta k_0 z - \int_0^z K_\Lambda(z')dz'\right]}A_i \\ q_s &= \sqrt{\frac{n_s}{\omega_s}}e^{-\frac{i}{2}\left[\Delta k_0 z - \int_0^z K_\Lambda(z')dz'\right]}A_s \end{aligned} \tag{4}$$

Equations (1) and (2) can be simplified to a dimensionless SU(2) symmetry [10], [39] as:

$$\frac{\partial}{\partial\tau}\begin{pmatrix} q_i \\ q_s \end{pmatrix} = i\begin{bmatrix} \Delta(\tau) & g(\tau)e^{-i\phi(\tau)} \\ g(\tau)e^{i\phi(\tau)} & -\Delta(\tau) \end{bmatrix}\begin{pmatrix} q_i \\ q_s \end{pmatrix} \tag{5}$$

with the following rescaling definitions:

$$\begin{aligned} I &= |q_i|^2 + |q_s|^2 \\ A_p &= |A_p|e^{i\phi_p} \equiv const \\ d_{eff} &= \frac{d_{ij}}{c\pi} \\ \eta &= 4d_{eff}|A_p|\sqrt{\frac{\omega_i\omega_s}{n_i n_s}} \\ \tau &= \eta z \\ g(\tau) &= \sin[\pi D(z)] \\ \Delta(\tau) &= \frac{\Delta k_0 - K_\Lambda(\tau)}{2\eta} \\ \phi(\tau) &= \phi_p - \phi_d(\tau) \end{aligned} \tag{6}$$

where I is the total photon flux of idle and signal light. Here, we assume that the pump is nearly lossless in the whole conversion process, so $A_p \equiv const$. For convenience, the initial inputs of idler and signal light are set to $q_i(0) = 1$ and $q_s(0) = 0$, respectively. In addition, d_{eff} is the normalized first-order QPM modulation strength, η is the rescaling coefficient to the length of the crystal, τ is the dimensionless time coordinate, $g(\tau)$ is the effective duty cycle, $\Delta(\tau)$ is the effective modulation wave vector, and $\phi(\tau)$ is the phase of the QPM parameter. Subsequently, we numerically calculate the relevant parameters. The idler, signal and pump wavelengths are chosen as $\lambda_i = 600\,\mathrm{nm}$, $\lambda_s = 432.6\,\mathrm{nm}$, and $\lambda_p = 1550\,\mathrm{nm}$, respectively. The idler wave is incident on a $LiNbO_3 (d_{ij} = 27\,\mathrm{pm/V})$ crystal of centimetre scale length, pumped with a uniform intensity of $I_p = 100\,\mathrm{mW/cm^2}$.

The variation in these three QPM parameters can be denoted by the motion of a vector $\boldsymbol{Q} = (g\cos\phi, g\sin\phi, \Delta)$ in the parameter space; see Figs. 1 and 2.

III. Geometrical Representation and Calculation

To describe the geometric motion of (5), we define a parameter space for the QPM vector as $(X_Q, Y_Q, Z_Q) =$

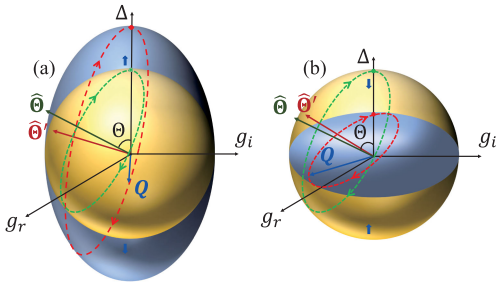

Fig. 1. (a, b) Trajectories of vector Q on the surfaces of spheres in the QPM parameter space. The circular rotation (green dashed curves) on the Bloch sphere (yellow sphere) is stretched or compressed longitudinally (Δ-axis direction) to form elliptical rotation (red dashed curves). Here, Θ is the angle between the normal vector $\hat{\Theta}$ of the trajectory plane and the Δ axis. $\hat{\Theta}'$ is the new normal vector of the trajectory surface after the deformation of the sphere. (a) Prolate spheroid (blue one) formed by longitudinal stretching of the Bloch sphere, in which the ratio of the length of axes is $(g_r : g_i : \Delta) = (1:1:1.5)$, and the oblateness α of the ellipsoid is 0.33. (b) Oblate spheroid (blue one) formed by longitudinally compressing the Bloch sphere, in which the ratio of the length of axes is $(g_r : g_i : \Delta) = (1:1:0.5)$, and the oblateness α of the ellipsoid is 0.5.

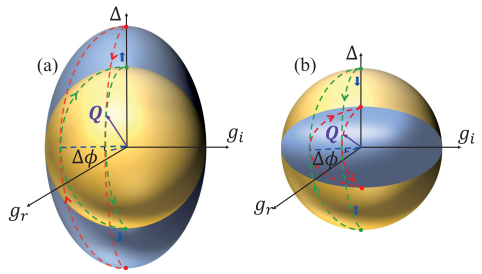

Fig. 2. (a, b) Elliptical wedge trajectories (red dashed curves) of vector Q on the surfaces of two ellipsoids in the QPM parameter space. Here, $\Delta\phi$ is the wedge angle. (a) Prolate spheroid with axial length ratio of $1:1:1.5$, and the oblateness α of the ellipsoid is 0.33. (b) Oblate spheroid with axial length ratio of $1:1:0.5$, and the oblateness α of the ellipsoid is 0.5.

$(g\cos\phi, g\sin\phi, \Delta)$. In this paper, we consider the vector Q to follow elliptical rotation and elliptical wedge rotation.

A. Elliptical Rotation

The elliptical rotation of vector Q can be constructed as [32]:

$$\begin{aligned}\Delta(\tau) &= \kappa(\sin^2\Theta\cos\omega\tau + \cos^2\Theta)\\ g(\tau) &= \sqrt{1-(\sin^2\Theta\cos\omega\tau+\cos^2\Theta)^2}\\ \phi(\tau) &= \arctan\frac{\sin\omega\tau}{\cos\Theta(1-\cos\omega\tau)}\end{aligned} \tag{7}$$

In the above formula, Θ is the angle between the normal vector of the elliptical trajectory plane and the Δ-axis, $0 \le \Theta \le \pi/2$; ω is the angular velocity, which satisfies $\omega = 2\pi/T$ ($T = \eta L$ is the period of modulation, and L is the crystal length). In addition, κ is a variable modulation wave vector coefficient, which can control the compression or stretching of the long axis of the Bloch sphere and then change the evolution trajectory of the QPM parameters (see Fig. 1). Fig. 1(a) shows the trajectory variation diagram on the surface of the sphere after longitudinal stretching when the modulation wave vector coefficient, κ, changes from 1 to 1.5, while Fig. 1(b) shows the trajectory variation diagram of the sphere after compression when κ changes from 1 to 0.5. The circular rotation (green dashed curve) on the Bloch sphere changes to an elliptical rotation (red dashed curve). Fig. 1 shows the misalignment of the normal vector $\hat{\Theta}$ after the Bloch sphere has been deformed.

B. Elliptical Wedge Rotation

For the elliptical wedge rotation, the trajectory of vector Q can be defined as [38]:

$$\begin{aligned}\Delta(\tau) &= \kappa\cos\omega\tau\\ g(\tau) &= |\sin\omega\tau|\\ \phi(\tau) &= H(\tau - T/2)\Delta\phi\end{aligned} \tag{8}$$

where $H(\tau - T/2)$ is the Heaviside step-function. $\Delta\phi$ is the wedge angle. Similarly, when the sphere is stretched (see Fig. 2(a)) or compressed (see Fig. 2(b)) by adjusting κ, the wedge rotation (green dashed curve) formed by the vector Q on the sphere also becomes an elliptical wedge rotation (red dashed curve). All trajectories on different spheres have the same wedge angle $\Delta\phi$.

C. Calculation of the AGP

When light propagates along a periodically modulated crystal, in addition to the inherent dynamic phase $\mathcal{D}$, it also produces a geometric phase γ that depends on the geometric properties of the path [40]. For the system, the dynamic phase can be obtained by the integral of the eigenvalue of the system in the whole evolution, which is defined as:

$$\mathcal{D} = \int_0^L \mu d\tau \tag{9}$$

Here, $\mu = \sqrt{\Delta(\tau)^2 + g(\tau)^2}$ is the eigenvalue of the symmetric matrix in (5). By replacing the definitions of $\Delta(\tau)$ and $g(\tau)$ of the two rotation schemes into it, we can obtain the expression of μ. Then, the geometric phase γ can be obtained by subtracting the dynamic phase $\mathcal{D}$ from the total phase Φ:

$$\gamma = \Phi - \mathcal{D} \tag{10}$$

D. Results and Discussion

For a set of known parameters, (Δ, g, ϕ), we can design a certain geometric phase plate. When the input beams propagate along the plate, the geometric phase accumulates. Then, the current problem is how to select an appropriate angle (Θ or $\Delta\phi$) to make the geometric phase more robust. Therefore, we need to study how these angles affect the accumulation of the geometric phase.

When $\kappa = 1$, the geometric phase generated in the circular rotation scheme satisfies [32], [34], [36]:

$$\gamma = -\pi(1 - \cos\Theta) \tag{11}$$

By adjusting the value of κ, the sphere is stretched or compressed into an ellipsoid, and the trajectory of vector $\boldsymbol{Q}$ on it becomes an ellipse. In this situation, the curve of the accumulated geometric phase with respect to the angle Θ no longer conforms

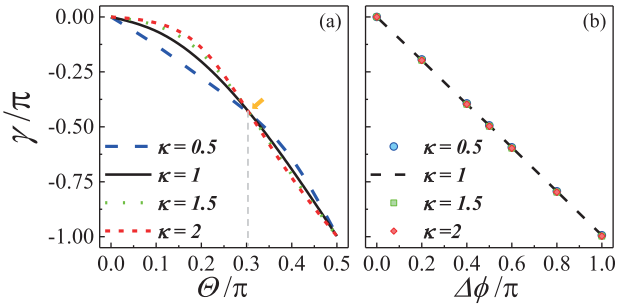

Fig. 3. (Color online) (a, b) Geometric phase, γ/π, versus the angles, Θ/π and $\Delta\phi/\pi$, under different modulation vector coefficients, κ. Here, $\kappa = 0.5, 1, 1.5, 2$. (a) Θ is the angle between the normal vector of the elliptical trajectory plane and the Δ-axis. (b) $\Delta\phi$ is the wedge angle.

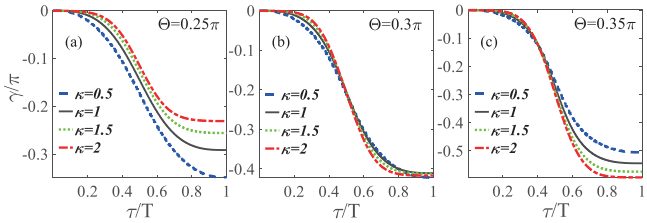

Fig. 4. Typical example of geometric phase accumulation at a specific angle, Θ, on an elliptical modulated crystal. (a, b, c) Geometric phase, γ/π, versus the time coordinate, τ/T, with different κ values, where the angles, Θ, are 0.25π, 0.3π, and 0.35π.

to (11). The results are shown in Fig. 3(a). All the $\gamma(\Theta)$ curves of different κ values separate, but they intersect at a common angle of Θ (approximately 0.3π). Typical examples of the geometric phase accumulated near the specific angle, $\Theta = 0.3\pi$, are shown in Fig. 4. We selected three values of Θ, which are located on the left ($\Theta = 0.25\pi$, see Fig. 4(a)), near ($\Theta = 0.3\pi$, see Fig. 4(b)) and right ($\Theta = 0.35\pi$, see Fig. 4(c)) of the intersection. In Fig. 4(a) and (c), the accumulated geometric phase at the end of the crystal shows clear divergence under different values of κ. Although there is some divergence at different positions of the crystal for various shapes of the Bloch sphere, the curves reach nearly the same point after the light travels through the whole nonlinear crystal (see Fig. 4(b)).

Therefore, we can conclude that when the QPM vector undergoes elliptical rotation, the accumulation of the geometric phase is related to the oblateness (determined by the length of the long axis, κ) of the ellipsoid. However, under different values of oblateness, there is a constant geometric phase, which is located at $\Theta \approx 0.3\pi$. This means that variable selection at this point is more flexible, while other points do not have this feature. To make the accumulation of the geometric phase more controllable, we consider the elliptical wedge rotation scheme.

For the wedge trajectory, when $\kappa = 1$, the geometric phase satisfies [32], [38]:

$$\gamma = -\Delta\phi \tag{12}$$

Our research shows that when κ changes, the accumulated geometric phase does not change, and the $\gamma(\Theta)$ curves still satisfy (12). The results are shown in Fig. 3(b). Typical examples of geometric phase accumulation at a specific angle, $\Delta\phi$, on an elliptical modulated crystal are shown in Fig. 5. The results show perfect consistency.

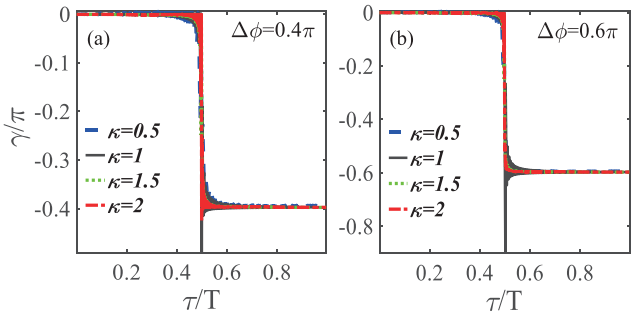

Fig. 5. Typical example of geometric phase accumulation at a specific angle, $\Delta\phi$, on an elliptical wedge-modulated crystal. (a-b) Geometric phase, γ/π, versus the time coordinate, τ/T, with different values, where the angles, $\Delta\phi$, are 0.4π and 0.6π, respectively.

In fact, previous studies have shown that the geometric phase γ is related to the solid angle Ω surrounded by the trajectory on the sphere [24], [32], [40]. The result of elliptical rotation is inconsistent because the solid angle of the trajectory surface changes after stretching or compressing the sphere, while Ω in the elliptical wedge rotation remains invariant. According to the definition of the solid angle, $\Omega = S/R^2$ (where S is the area enclosed by the closed trajectory and R is the distance from the trajectory surface to the center of the sphere), we calculate the solid angle surrounded by the wedge trajectory corresponding to the same wedge angle $\Delta\phi$ in sphere Ω_s and ellipsoid Ω_e.

The solid angle Ω_s in the sphere satisfies:

$$\Omega_s = \frac{4\pi r^2}{r^2}\frac{\Delta\phi}{2\pi} = 2\Delta\phi \tag{13}$$

and Ω_e satisfies:

$$\Omega_e = \frac{4\pi R^2}{R^2}\frac{\Delta\phi}{2\pi} = 2\Delta\phi \tag{14}$$

where $R = \sqrt{\frac{ab+bc+ac}{3}}$, where a, b, c are the three axial lengths of an ellipsoid. This theoretically explains why the simulation results are the same.

In addition, comparing the results in the two schemes, we find that there is a point of correlation between the elliptical wedge and the elliptical trajectory, i.e., $\Theta = \pi/2$. At this point, the normal vector $\hat{\mathbf{\Theta}}$ of the elliptical trajectory lies on the equator as in the elliptical wedge scheme, when a longitudinal change in the sphere does not change the direction of the normal vector. Instead, there is a spatial rotation (see Fig. 1) at the remaining positions, which in turn causes a change in the accumulation of geometric phases. This illustrates the robustness of the wedge rotation.

Indeed, limited by the current level of polarization, it is still challenging to control all three variables: modulation wave vector, duty cycle and modulation phase, simultaneously on a centimetre-sized crystal, so that they obey a specific relationship. In terms of scheme design, the design of the function for the elliptical rotation scheme is more complex than for the elliptical wedge scheme. If there is an error in one of the variables (in

the case of the modulated wave vector), according to the results of this paper, it does not affect the wedge scheme, but clearly affects the results of the circular scheme. This also reflects the significance of our study.

IV. Conclusion

The purpose of this work is to create a robust and well-predicted geometric phase in the three wave mixing process with an undepleted pump approximation by changing the coefficient κ of the modulated wave vector Δ, which is one of the quasi-phase-matching parameters. We find that the AGPs corresponding to two typical parameter trajectories have different performances when the Bloch sphere is deformed. Compared with the elliptical rotation, the results in the elliptical wedge rotation are more flexible, and the accumulated AGPs do not depend on the shape of the sphere. Previous studies have shown that the magnitude of AGP is related to the solid angle of the closed surface. Based on this result, we calculate the solid angle surrounded by the trajectory surface on the Bloch sphere and find that the solid angle in the elliptical wedge scheme remains fixed during the stretching or compression of the axis length of the sphere. In addition, we also find that although the geometric phases in the elliptical rotation depend on the wave vector parameters as a whole, there is an intersection point where the AGPs are fixed at a certain value. The result is also related to the change in the solid angle, but what kind of change has taken place needs further research and summary. Moreover, there is one point where two schemes are degenerate, i.e., $\Theta = \pi/2$ corresponding to $\Delta\phi = \pi$.

In short, the geometric phase provides a unified description of a wide range of phenomena in quantum physics and nonlinear optics, and its robust controllability is of great significance for many fields, examples include geometric phase-based lenses [41], wavefront surface tailoring [42], [43], intracavity laser shaping of structured beams [44], the improvement of the depth-of-field in microscopy [45], even a new approach to generate entangled photons [46]. We believe that the results of this study can provide some reference and guidance for geometric phase manipulation experiments using photonic devices.

References

[1] A. Rundquist *et al.*, "Phase-matched generation of coherent soft X-rays," *Science*, vol. 280, no. 5368, pp. 1412–1415, 1998.

[2] Y. Tamaki *et al.*, "Highly efficient, phase-matched high-harmonic generation by a self-guided laser beam," *Phys. Rev. Lett.*, vol. 82, no. 7, pp. 1422–1425, 1999.

[3] D. Lu *et al.*, "Validation of the angular quasi-phase-matching theory for the biaxial optical class using PPRKTP," *Opt. Lett.*, vol. 43, no. 17, pp. 4276–4279, 2018.

[4] J. A. Giordmaine, "Mixing of light beams in crystals," *Phys. Rev. Lett.*, vol. 8, no. 1, pp. 19–20, 1962.

[5] R. W. Boyd, *Nonlinear Optics*, New York, NY, USA: Academic, 2008, pp. 69–104.

[6] A. Arie and N. Voloch, "Periodic, quasi-periodic, and random quadratic nonlinear photonic crystals," *Laser Rev.*, vol. 4, no. 3, pp. 355–373, 2010.

[7] D. S. Hum and M. M. Fejer, "Quasi-phasematching," *Comptes Rendus Physique*, vol. 8, no. 2, pp. 180–198, 2007.

[8] C. R. Phillips and M. M. Fejer, "Efficiency and phase of optical parametric amplification in chirped quasi-phase-matched gratings," *Opt. Lett.*, vol. 35, no. 18, pp. 3093–3095, 2010.

[9] B. W. Mayer, C. R. Phillips, L. Gallmann, and U. Keller, "Mid-infrared pulse generation via achromatic quasi-phase-matched OPCPA," *Opt. Exp.*, vol. 22, no. 17, pp. 20798–20808, 2014.

[10] H. Suchowski, G. Porat, and A. Arie, "Adiabatic processes in frequency conversion," *Laser Rev.*, vol. 8, no. 3, pp. 333–367, 2014.

[11] D. D. Hickstein *et al.*, "High-harmonic generation in periodically poled waveguides," *Optica*, vol. 4, no. 12, pp. 1538–1544, 2017.

[12] H. Suchowski *et al.*, "Robust adiabatic sum frequency conversion," *Opt*., vol. 17, no. 15, pp. 12731–12740, 2009.

[13] G. Porat and A. Arie, "Efficient, broadband, and robust frequency conversion by fully nonlinear adiabatic three-wave mixing," *J. Opt. Soc. Amer. B*, vol. 30, no. 5, pp. 1342–1351, 2013.

[14] B. Chen, L. Hong, C. Hu, and Z. Li, "White laser realized via synergic second- and third-order nonlinearities," *Research*, vol. 2021, 2021, Art. no. 1539730.

[15] T. Wan, T. Wang, H. Zhang, and C. Chen, "The synthesis of white-laser source based on the frequency conversion with the stark-chirped rapid adiabatic passage," *Results Phys.*, vol. 22, Mar. 2021, Art. no. 103871.

[16] P. Krogen *et al.*, "Generation and multi-octave shaping of mid-infrared intense single-cycle pulses," *Nature Photon.*, vol. 11, no. 4, pp. 222–226, 2017.

[17] H. Suchowski *et al.*, "Adiabatic frequency conversion of ultrafast pulses," *Appl. Phys. B*, vol. 105, no. 4, pp. 697–702, 2011.

[18] J. Moses, H. Suchowski, and F. X. Kärtner, "Fully efficient adiabatic frequency conversion of broadband Ti: Sapphire oscillator pulses," *Opt. Lett.*, vol. 37, no. 9, pp. 1589–1591, 2012.

[19] D. Wei *et al.*, "Multiple generations of high-order orbital angular momentum modes through cascaded third-harmonic generation in a 2D nonlinear photonic crystal," *Opt. Exp.*, vol. 25, no. 10, pp. 11556–11563, 2017.

[20] Y. Wu *et al.*, "Tunable third harmonic generation of vortex beams in an optical superlattice," *Opt. Exp.*, vol. 25, no. 25, pp. 30820–30826, 2017.

[21] F. Eilenberger, M. Bache, S. Minardi, and T. Pertsch, "Temporal switching induced by cascaded third order nonlinearity," *Opt. Lett.*, vol. 37, no. 24, pp. 5109–5111, 2012.

[22] M. Bache, F. Eilenberger, and S. Minardi, "Higher-order Kerr effect and harmonic cascading in gases," *Opt. Lett.*, vol. 37, no. 22, pp. 4612–4614, 2012.

[23] P. Margules, J. Moses, H. Suchowski, and G. Porat, "Ultrafast adiabatic frequency conversion," *J. Phys*., vol. 3, Apr. 2021, Art. no. 022011.

[24] M. V. Berry, "Quantal phase factors accompanying adiabatic changes," *Proc. Roy. Soc. London A*, vol. 392, pp. 45–57, 1984.

[25] J. Fan, T. Lei, and X. Yuan, "Active near-infrared wavefront engineering employing geometric phase metasurfaces combined with phase-change materials," *J. Phys. D: Appl. Phys.*, vol. 54, May 2021, Art. no. 285105.

[26] T. Zhan *et al.*, "Fabrication of Pancharatnam–Berry phase optical elements with highly stable polarization holography," *Opt. Exp.*, vol. 27, no. 3, pp. 2632–2642, 2019.

[27] Z. Bomzon, V. Kleiner, and E. Hasman, "Pancharatnam-berry phase in space-variant polarization-state manipulations with subwavelength gratings," *Opt. Lett.*, vol. 26, no. 18, pp. 1424–1426, 2001.

[28] L. Marrucci, C. Manzo, and D. Paparo, "Pancharatnam-berry phase optical elements for wave front shaping in the visible domain: Switchable helical mode generation," *Appl. Phys. Lett.*, vol. 88, May 2006, Art. no. 221102.

[29] Y. Yuana *et al.*, "Terahertz dual-band polarization control and wavefront shaping over freestanding dielectric binary gratings with high efficiency," *Opt. Laser Eng.*, vol. 143, Mar. 2021, Art. no. 116636.

[30] Q. Song *et al.*, "Broadband decoupling of intensity and polarization with vectorial Fourier metasurfaces," *Nature Commun.*, vol. 12, Jun. 2021, Art. no. 3631.

[31] R. Hayward and F. Biancalana, "Complex Berry phase dynamics in PT-symmetric coupled waveguides," *Phys. Lett. A*, vol. 98, Nov. 2018, Art. no. 053833.

[32] A. Karnieli and A. Arie, "Fully controllable adiabatic geometric phase in nonlinear optics," *Opt. Exp.*, vol. 26, no. 4, pp. 4920–4932, 2018.

[33] A. Karnieli, S. T. Mills, G. D. Domenico, and A. Arie, "Experimental observation of the geometric phase in nonlinear frequency conversion," *Optica*, vol. 6, no. 11, pp. 1401–1405, 2019.

[34] Y. Li *et al.*, "Adiabatic geometric phase in fully nonlinear three-wave mixing," *Phys. Rev. A*, vol. 101, Mar. 2020, Art. no. 033807.

[35] Y. Li, J. Lü, S. Fu, and A. Arie, "Geometric representation and the adiabatic geometric phase in four-wave mixing processes," *Opt. Exp.*, vol. 29, no. 5, pp. 7288–7306, 2021.

[36] J. L, F. Zhao, W. Pang, and Y. Li, "Constant adiabatic geometric phase in three-wave mixing under different depletion levels," *Phys. Lett. A*, vol. 397, May 2021, Art. no. 127266.
[37] C. P. Jisha, A. Alberucci, J. Beeckman, and S. Nolte, "Self-trapping of light using the Pancharatnam–Berry phase," *Phys. Rev. X*, vol. 9, no. 2, 2019, Art. no. 021051.
[38] F. Zhao *et al.*, "Geometric phase with full-wedge and half-wedge rotation in nonlinear frequency conversion," *Opt. Express*, vol. 29, no. 14, pp. 21820–21832, 2021.
[39] R. Bhandari, "Polarization of light and topological phases," *Phys. Rep*. vol. 281, pp. 1–64, 1997.
[40] S. Pancharatnam, "Generalized theory of interference and its applications," *Proc. Ind. Acad. Sci.—Sec. A*, vol. 44, no. 5, pp. 247–262, 1956.
[41] C. P. Jisha, S. Nolte, and A. Alberucci, "Geometric phase in optics: From wavefront manipulation to waveguiding," *Laser Rev.*, vol. 15, no. 10, 2021, Art. no. 2100003.
[42] M. Tal, D. B. Haim, and T. Ellenbogen, "Geometric phase opens new frontiers in nonlinear frequency conversion of light," *Front. Phys.*, vol. 17, 2022, Art. no. 12302.
[43] A. Karnieli, Y. Li, and A. Arie, "The geometric phase in nonlinear frequency conversion," *Front. Phys.*, vol. 17, no. 1, 2022, Art. no. 12301.
[44] A. Forbes, "Structured light from lasers," *Laser Rev.*, vol. 13, no. 11, 2019, Art. no. 1900140.
[45] F. Cardano and L. Marrucci, "Spin-orbit photonics," *Nature Photon.*, vol. 9, pp. 776–778, 2015.
[46] F. Flamini, N. Spagnolo, and F. Sciarrino, "Photonic quantum information processing: A review," *Rep. Prog. Phys.*, vol. 82, no. 1, 2015, Art. no. 016001.